Journal of Solid State Chemistry 183 (2010) 168–172

Contents lists available at ScienceDirect

Journal of Solid State Chemistry

journal homepage: www.elsevier.com/locate/jssc

Antiferromagnetism of perovskite $EuZrO_3$

Yanhua Zong, Koji Fujita *, Hirofumi Akamatsu, Shunsuke Murai, Katsuhisa Tanaka

Department of Material Chemistry, Graduate School of Engineering, Kyoto University, Katsura, Nishikyo-ku, Kyoto 615-8510, Japan

ARTICLE INFO

Article history:
Received 22 July 2009
Received in revised form
19 October 2009
Accepted 22 October 2009
Available online 29 October 2009

Keywords:
Orthorhombic perovskite
Europium zirconate
Antiferromagnetism
Magnetic interaction
Mössbauer spectroscopy

ABSTRACT

Polycrystalline $EuZrO_3$ has been synthesized by the solid-state reaction between EuO and ZrO_2, and its structural and magnetic properties have been investigated. Rietveld analysis of the X-ray diffraction pattern indicates that $EuZrO_3$ crystallizes in an orthorhombic perovskite structure. ^{151}Eu Mössbauer effect measurement reveals that almost all the europium ions are present as the divalent state and occupy distorted sites with non-axial electric field gradients, in agreement with the orthorhombic structure. In contrast to previous reports, an antiferromagnetic transition was observed around 4.1 K. The magnetic structure below the Néel temperature has been discussed.

1. Introduction

Divalent europium (Eu^{2+})-bearing perovskite oxides, $EuM^{4+}O_3$ (e.g. M=Ti, Nb), have been studied in the last several decades for their intriguing magnetic and electrical properties [1–7]. A variety of magnetic and electrical properties has been observed, depending on the kind of M cations, oxygen non-stoichiometry, and aliovalent cationic substitution. For instance, europium niobate ($EuNbO_3$) behaves like a ferromagnetic (FM) metal [1,2], while the introduction of oxygen vacancies converts it into a superconductor with a critical temperature of about 6 K [3]. On the other hand, europium titanate ($EuTiO_3$) is an antiferromagnetic (AFM) insulator with a Néel temperature (T_N) of about 5.5 K, and quantum paraelectric properties with strong spin–lattice coupling are observed at low temperatures [4–7]. Our recent experimental results have demonstrated that the AFM state of $EuTiO_3$ is converted into a FM state through the lattice expansion in epitaxial thin films [8], which is in good agreement with the theoretical prediction proposed by Ranjan et al. [6]. In addition, it has been reported that partial substitution of trivalent rare-earth ions (e.g. La^{3+}, Gd^{3+}) for Eu^{2+} ions in $EuTiO_3$ introduces electrons into the conduction band of Ti 3d states, resulting in the occurrence of FM metals [9].

Compared with $EuNbO_3$ and $EuTiO_3$, the structure and physical properties of europium zirconate ($EuZrO_3$) have been less investigated. Shafer [10] first prepared $EuZrO_3$ by a high-temperature solid-state reaction using ZrO_2 and EuO as starting materials and ascribed its crystal structure to a cubic perovskite. Recently, Viallet et al. [11] performed X-ray diffraction (XRD) pattern refinement on $EuZrO_3$ prepared by the same procedure in Ref. [10] and showed that it crystallizes in orthorhombic symmetry at room temperature. Namely, the previous reports on the crystal structure of $EuZrO_3$ are quite controversial. In addition, the magnetic ordering of $EuZrO_3$ has not been observed down to 4 K [10,11] which was the lowest measurement temperature. Therefore, further investigation is necessary to clarify both the crystal structure and magnetism of $EuZrO_3$.

In this study, we have synthesized polycrystalline $EuZrO_3$ following the method described in Refs. [10,11], and examined its crystal structure and magnetic properties. Almost all europium ions are present as the divalent state in the synthesized $EuZrO_3$, as revealed by ^{151}Eu Mössbauer spectroscopy. The crystal structure is refined to an orthorhombic perovskite-type structure (*Pbnm* space group) through Rietveld analysis of the XRD pattern. In contrast to previous reports, measurements of magnetic susceptibility down to 2 K demonstrate that orthorhombic perovskite $EuZrO_3$ behaves as an antiferromagnet below about 4.1 K. This is the first observation of magnetic ordering in $EuZrO_3$.

2. Experimental procedures

Polycrystalline $EuZrO_3$ was prepared from reagent-grade Eu_2O_3, ZrO_2, and graphite powders through the following two processes: (I) $Eu_2O_3+C \rightarrow CO+2EuO$; and (II) $EuO+ZrO_2 \rightarrow EuZrO_3$. In the first step, Eu_2O_3 and slightly excessive graphite were thoroughly mixed and pressed into a pellet. The pellet was then sintered at 1450 °C for 6 h in an Ar(95)/H_2(5) (vol%) atmosphere.

* Corresponding author.
E-mail address: fujita@dipole7.kuic.kyoto-u.ac.jp (K. Fujita).

0022-4596/$ - see front matter © 2009 Elsevier Inc. All rights reserved.
doi:10.1016/j.jssc.2009.10.014

Although the XRD pattern of the resultant product (not shown) revealed the presence of a minor impurity phase identified as Eu_3O_4 (~3.9 wt%), the major crystalline phase was EuO. In the second step, the resultant EuO pellet was reground into powder and thoroughly mixed with ZrO_2. The mixture was again pressed into a pellet and sintered at 1550 °C for 10 h in the Ar(95)/H_2(5) (vol%) atmosphere.

Powder XRD patterns were recorded on a Rigaku Rint 2500 X-ray diffractometer with Cu$K\alpha$ radiation (λ=1.5406 Å). Rietveld analysis was performed by a least-square method using the GSAS refinement program [12]. The lattice constants, atomic coordinates, occupation factors, and isotropic thermal parameters were refined freely for all atoms. Crystal structure of $EuZrO_3$ was drawn with the refined parameters using the VESTA software [13]. In order to evaluate the valence state of europium ions and the local environment around Eu^{2+} ions, ^{151}Eu Mössbauer effect measurements were performed in a standard transmission geometry at room temperature using $^{151}Sm_2O_3$ with activity of 1.85 GBq as a 21.5 keV γ-ray source. The velocity calibration was done with the magnetic hyperfine spectrum of α-Fe foil obtained using ^{57}Co-doped Rh as a 14.4 keV γ-ray source. The Mössbauer spectrum of EuF_3 was measured as a standard of Doppler velocity. As a reference, we also measured the Mössbauer spectrum of EuS with rock-salt structure in order to determine the full width at half maximum (FWHM) of Eu^{2+} absorption peak in cubic symmetry; the FWHM was estimated to be about 2.5 mm/s for our γ-ray source. Magnetization measurements were carried out with a superconducting quantum interference device (SQUID) magnetometer (MPMS2, Quantum Design). The temperature dependence of magnetic susceptibilities was measured in a range of 2–300 K under both zero-field-cooling (ZFC) and field-cooling (FC) conditions at an external magnetic field of 50 Oe. The field dependence of magnetization was recorded at 2 K under magnetic fields up to 5 T.

3. Results and discussion

3.1. Crystal structure

Fig. 1 shows the XRD pattern of the polycrystalline $EuZrO_3$ sample at room temperature (open circles). All the diffraction peaks can be indexed as an orthorhombic perovskite phase (*Pbnm* space group), which is consistent with the result reported by Viallet et al. [11] but not with that by Shafer [10]. Utilizing the orthorhombic structure of $SrZrO_3$ as a starting model, Rietveld refinement was performed, yielding an overall good agreement between the observed and calculated diffraction profiles (solid line). The final refinement converged to R_{wp}=7.8%, R_p=5.2%, and χ^2=1.92. The R_p factor is much smaller than that in Ref. [11] (11.9%). Some structural parameters deduced from the Rietveld refinement are summarized in Tables 1 and 2. The refined lattice constants, a=5.79469(9), b=5.82521(7), and c=8.19799(14) Å, are close to those reported in Ref. [11]. A view of the crystal structure of $EuZrO_3$ is illustrated in Fig. 2(a). The structure shows a $GdFeO_3$-type distortion through the rotation of ZrO_6 octahedra, due to the smaller size of Eu^{2+} ion compared with the cubo-octahedral interstice formed by the corner-sharing ZrO_6 network. The rotating angles in a–b plane (Φ) and normal to a–b plane (Θ) are estimated to be 6.2° and 12.7°, respectively, as shown in Figs. 2(b) and (c). The degree of the structure distortion of ABO_3-type perovskites can be evaluated by the tolerance factor, $t = <A-O>/\sqrt{2}<B-O>$, where $<A-O>$ and $<B-O>$ represent the mean cation–oxygen interatomic distances in the A- and B-site, respectively [14]. Geometrically, t equals to 1 for an ideal (cubic) perovskite. For $EuZrO_3$ where Eu^{2+} and Zr^{4+} ions occupy the A- and B-site, respectively, t is estimated to be 0.983, which again suggests a certain distortion from ideal perovskite structure.

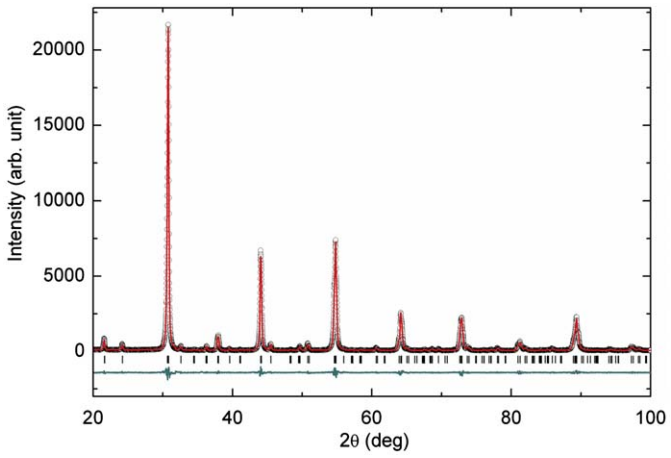

Fig. 1. Powder XRD pattern of $EuZrO_3$ synthesized by the solid-state reaction between EuO and ZrO_2 (open circles). The solid line represents the profile calculated by the Rietveld refinement. Vertical ticks indicate the expected reflection positions for the orthorhombic $EuZrO_3$. The bottom curve is the difference between experimental and calculated profiles.

3.2. ^{151}Eu Mössbauer spectroscopy

Fig. 3 shows the room-temperature ^{151}Eu Mössbauer spectrum of $EuZrO_3$. Two peaks are observed around −13 and 0.5 mm/s, assigned to Eu^{2+} and Eu^{3+} absorption, respectively. From the area ratio of the two absorption peaks, the fraction of Eu^{2+} relative to the total europium ions was estimated to be about 0.96. Since the effective Debye temperature of Eu^{2+} is usually lower than that of Eu^{3+} (e.g. 195 K for Eu^{2+} and 220 K for Eu^{3+} in $EuPd_3S_4$ [15], and 145 K for Eu^{2+} and 261 K for Eu^{3+} in fluorozirconate glass [16]), the real fraction of Eu^{2+} could be higher than 0.96. The fraction of Eu^{2+} in the present sample is comparable to those in $EuZrO_3$ and $EuTiO_3$ as reported previously [5,10]. A close look at Fig. 3 reveals that the Eu^{2+} absorption peak is asymmetrically broadened with a shoulder around −11.5 mm/s, suggesting the presence of electric quadrupole interaction between the electric field gradient and the electric quadrupole moment of ^{151}Eu nucleus. Since the fit of asymmetric Mössbauer spectrum with a single Lorentzian gives rise to a significant error in isomer shift value [17], we have utilized the method developed by Shenoy and Dunlap for analysis of pure quadrupole spectra [18]. In their method, the γ-ray resonance energy between (I^*, I_z^*) and (I, I_z) is given by

$$R(I_z^*, I_z) = eV_{zz}[Q_e P(I^*, I_z^*) - Q_g P(I, I_z)] + \delta, \quad (1)$$

Table 1
Atomic coordination, site occupancy, and isotropic thermal factors (U_{iso}) for orthorhombic $EuZrO_3$.

	x	y	z	Occupancy	U_{iso} (Å^2)
Eu	0.00557(25)	0.52478(8)	0.25	0.988(1)	0.0183(2)
Zr	0	0	0	0.971(2)	0.0136(3)
O1	−0.0789(19)	−0.0115(9)	0.25	1.029(24)	0.0189(48)
O2	0.2171(13)	0.2798(11)	0.0458(11)	0.981(18)	0.0238(35)

Lattice constants (*Pbnm*): a=5.79469(9), b=5.82521(7), and c=8.19799(14) Å. Weighted profile R_{wp}=7.8%, profile R_p=5.2%, and reduced χ^2=1.92.

Table 2
Selected distances (Å) in $EuZrO_3$.

NN Eu–Eu (× 2)	4.1540(21)	NN Eu–O1	2.482(11)	NN Zr–O1 (× 2)	2.100(2)
NN Eu–Eu (× 2)	4.0630(20)	NN Eu–O1	2.745(5)	NN Zr–O2 (× 2)	2.093(7)
NN Eu–Eu (× 2)	4.10966(11)	NN Eu–O1	3.162(5)	NN Zr–O2 (× 2)	2.115(7)
Mean NN < Eu–Eu >	4.1089	NN Eu–O1	3.329(12)	Mean NN 〈Zr–O〉	2.103
NNN Eu–Eu (× 2)	5.7950(20)	NN Eu–O2 (× 2)	2.518(7)		
NNN Eu–Eu (× 2)	5.8252(7)	NN Eu–O2 (× 2)	2.755(8)		
NNN Eu–Eu (× 4)	5.6640(11)	NN Eu–O2 (× 2)	2.974(9)		
NNN Eu–Eu (× 4)	5.9535(11)	NN Eu–O2 (× 2)	3.438(8)		
Mean NNN 〈Eu–Eu〉	5.8092	Mean NN 〈Eu–O〉	2.924		

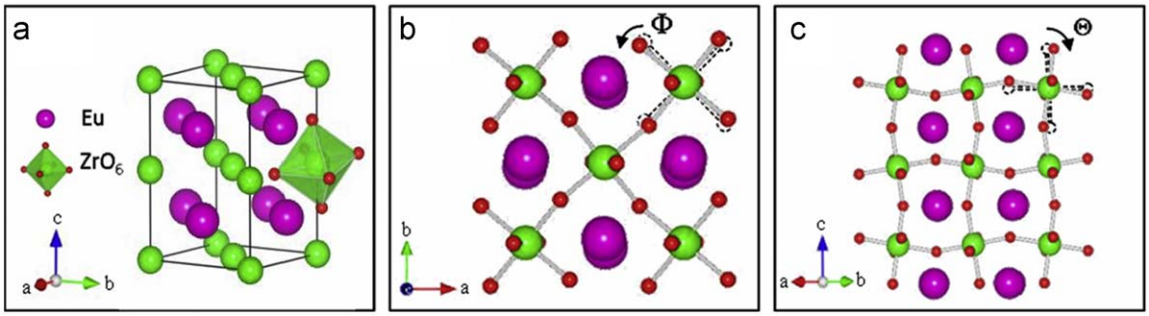

Fig. 2. (a) Crystal structure of $EuZrO_3$ drawn based on Rietveld refinement results. (b,c) Schematic illustration of the structure of $EuZrO_3$ projected along the [001] and [110] directions, respectively. The dashed lines indicate the corresponding positions of ZrO_6 octahedra in the ideal perovskite structure.

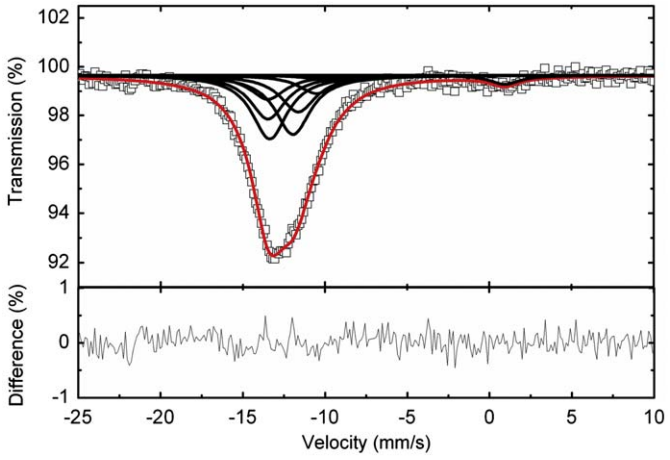

Fig. 3. Room-temperature Mössbauer spectrum of $EuZrO_3$ (open squares). The solid line represents the theoretical spectrum calculated by Eqs. (1)–(3) in which the presence of quadrupole interaction is considered. The component lines of the 12 transitions are also shown for the Eu^{2+} absorption peak at around −12 mm/s. The Eu^{3+} absorption peak at around 0.5 mm/s is simply analyzed by a single Lorenzian because of the poor shape resolution. The bottom curve is the difference between experimental and calculated profiles.

where e is the elementary charge, V_{zz} is the electric field gradient in the direction z, Q_e and Q_g are excited- and ground-state nuclear quadrupole moments, respectively, I^* and I are excited- and ground-state nuclear spins, respectively, I_z^* and I_z are z projections of excited- and ground-state nuclear spins, respectively, and δ is the isomer shift. $P(I^*, I_z^*)$ and $P(I, I_z)$ are written as

$$P(I, I_z) = \sum_{N=0}^{4} a_N(I, I_z)\eta^N, \tag{2}$$

where η is the asymmetry parameter of the electric field gradient, and $a_N(I, I_z)$ is the eigenvalue coefficient (see Ref. [18]). The transition intensity is expressed as

$$A(I^*, I_z^*, I, I_z) = \sum_{N=0}^{4} b_N(I^*, I_z^*, I, I_z)\eta^N, \tag{3}$$

where $b_N(I^*, I_z^*, I, I_z)$ is the intensity coefficient (see Ref. [18]). For ^{151}Eu, $I^*=7/2$, $I=5/2$, and $Q_e/Q_g=1.34$ [5]. Therefore, there are 12 possible transitions in the presence of quadrupole interactions. In calculation of the theoretical spectrum using Eqs. (1)–(3), we assume that each transition has a Lorentzian line shape with a FWHM of γ. In addition, we ignore magnetic hyperfine interaction because $EuZrO_3$ is paramagnetic at room temperature as described below. The fit of the theoretical curve to the Eu^{2+} absorption peak yields $\delta = -12.64 \pm 0.02$ mm/s, $eV_{zz}Q_g = -10.32 \pm 0.21$ mm/s, $\gamma = 2.65 \pm 0.05$ mm/s, and $\eta = 0.46 \pm 0.05$. The value of δ reflects the electron density at the nucleus [19]. For Eu^{2+}-containing ionic compounds, the δ value depends on the 6s electron density of Eu^{2+}, which is affected by the covalency of chemical bond between Eu^{2+} and the surrounding ligands and/or the coordination number of ligands for Eu^{2+} [20,21]. The δ value of $EuZrO_3$ is very close to that of cubic perovskite $EuTiO_3$ (-12.5 ± 0.1 mm/s) but slightly different from that of $EuZrO_3$ (-13.1 ± 0.2 mm/s) reported by Berkooz [21] (note that the values of δ reported in Ref. [21], which were relative to Eu_2O_3, are converted to those referred to EuF_3 by adding 1.037 mm/s to the original values). It is most probable that the difference in δ between the present $EuZrO_3$ and the one reported previously stems from the fact that the contribution of quadrupole interactions is taken into account in the present analysis; otherwise, the δ value is equal to the datum derived by Berkooz, corresponding exactly to the peak position of the Eu^{2+} absorption (see Fig. 3). Based on the above analyses of XRD pattern and Mössbauer spectrum, we believe that the δ value (-12.64 mm/s) obtained in this work is more reliable. On the other hand, the quadrupole interaction for Eu^{2+}-containing compounds mainly reflects the electric field gradient caused by the surrounding ligands because Eu^{2+} has a half-filled 4f-shell with nominally zero orbital angular momentum; namely, the anisotropy of 4f electrons is negligibly small [19]. The non-zero quadrupole interaction ($eV_{zz}Q_g = -10.32$ mm/s) and non-zero asymmetry parameter ($\eta = 0.46$) indicate the presence of non-axial electric field gradients at Eu^{2+} sites, consistent with the orthorhombic structure of $EuZrO_3$ where the Eu^{2+} sites have the point symmetry $m(C_{1h})$. The value of γ is almost the same as the

FWHM of absorption peak obtained for cubic EuS (2.5 mm/s), ensuring the occupation of single crystallographically equivalent sites by Eu^{2+} ions.

3.3. Magnetic properties

Fig. 4(a) illustrates the magnetic susceptibility (χ) as a function of temperature (T) measured for $EuZrO_3$ under the external magnetic field of 50 Oe. A kink structure corresponding to a magnetic transition is observed at 4.1 K without any divergence between ZFC and FC magnetic susceptibilities. The magnetization (M) as a function of external magnetic field (H) at 2 K is shown in Fig. 4(b). Since the Eu^{2+} ion has an S=7/2 spin with a Heisenberg character and least magnetic anisotropy, the Eu^{2+} spins are first flipped and then gradually changed into FM arrangement with increasing H. The magnitude of M tends to be saturated at higher H than 2 T. The saturation magnetization is 6.87μ_B, which is very close to the theoretical spin-only magnetic moment of Eu^{2+} (7μ_B). This result, together with the presence of kink structure in the χ–T curve, indicates the AFM order at the ground state.

We have analyzed the χ–T curve in the high-temperature region by considering both the Curie paramagnetism of Eu^{2+} and the Van Vleck paramagnetism of impurity Eu^{3+} ions:

$$\chi_{mol} = n\chi_{mol}(Eu^{2+}) + (1-n)\chi_{mol}(Eu^{3+}) + \chi_0, \quad (4)$$

where n is the molar ratio of Eu^{2+} to the total europium ions, and χ_0 is the temperature-independent term. According to the Curie–Weiss law, the magnetic susceptibility of Eu^{2+}, $\chi_{mol}(Eu^{2+})$, is represented by

$$\chi_{mol}(Eu^{2+}) = \frac{N_A(\mu_{eff})^2}{3k(T-\theta_W)}, \quad (5)$$

where N_A is Avogadro's number, μ_{eff} the effective magnetic moment of Eu^{2+}, k the Boltzmann constant, and θ_W the Weiss temperature. The ground state $^7F_0$ of Eu^{3+} is nonmagnetic, and the excited states ^7F_J (J=1, 2,…, 6) are so close to the ground state that the energy differences are comparable to kT at room temperature. In consideration of the first three excited states, the magnetic susceptibility of Eu^{3+}, $\chi_{mol}(Eu^{3+})$, can be calculated by the Van Vleck formula [22]:

$$\chi_{mol}(Eu^{3+}) = \frac{N_A\mu_B^2}{3kT} \times \frac{24/a + (13.5 - 1.5/a)e^{-a} + (67.5 - 2.5/a)e^{-3a} + (189 - 3.5/a)e^{-6a}}{1 + 3e^{-a} + 5e^{-3a} + 7e^{-6a}}, \quad (6)$$

where $a=\lambda/kT$ is the ratio of the multiplet width (λ is the spin–orbit coupling constant) to the thermal energy. If we take λ=370 cm^{-1} as reported for $EuAlO_3$ [23] and μ_{eff}=7.94μ_B as obtained theoretically, the experimental susceptibility can be well reproduced with Eqs. (4)–(6) (see the solid line in Fig. 4(a)), yielding n=0.97 and θ_W=+0.07 K. The value of n is very close to that obtained from the Mössbauer measurement. The AFM behavior with positive θ_W value implies the presence of FM interactions as well as the AFM interactions between localized Eu^{2+} spins in $EuZrO_3$.

In the final part, we will address the mechanism responsible for the observed AFM ordering in $EuZrO_3$. In Eu^{2+}-containing crystalline oxides with perovskite-type structure, the magnetic structure is predominantly determined by the nearest-neighbor (NN) and next-nearest-neighbor (NNN) exchange interactions between Eu^{2+} ions [4–6,24–26]. These exchange interactions are characterized by the exchange constants J_1 and J_2, respectively. For AFM perovskites where magnetic ions are located on a simple cubic lattice, there exist three types of AFM ordering, namely, A-, C-, and G-type (see Fig. 5), and the values of J_1 and J_2 can be derived from the following equations using the molecular-field approximation [26],

$$\theta_W = \frac{2S(S+1)}{3k}(6J_1 + 12J_2), \quad (7)$$

$$T_{N1} = \frac{2S(S+1)}{3k}(2J_1 - 4J_2), \quad (8)$$

$$T_{N2} = \frac{2S(S+1)}{3k}(2J_1 + 4J_2), \quad (9)$$

$$T_{N3} = \frac{2S(S+1)}{3k}(-6J_1 + 12J_2), \quad (10)$$

where T_{N1}, T_{N2}, and T_{N3} are the Néel temperatures for A-, C-, and G-type AFM ordering, respectively. In pseudocubic perovskite $EuZrO_3$, Eu^{2+} ions locate on an approximately cubic lattice. Disregarding the structure distortion and setting S=7/2, one obtains J_1/k=+0.033 K and J_2/k=−0.031 K for an A-type AFM structure using Eqs. (7) and (8), while the analysis on a G-type AFM structure using Eqs. (7) and (10) yields J_1/k=−0.032 K and J_2/k=+0.017 K. There is no solution by combining Eq. (7) with Eq. (9), so the possibility of the C-type AFM ordering can be ruled out for $EuZrO_3$. Although we do not have further experimental evidence to distinguish the A-type AFM structure from the G-type one for $EuZrO_3$ at this moment, previous analysis of magnetic

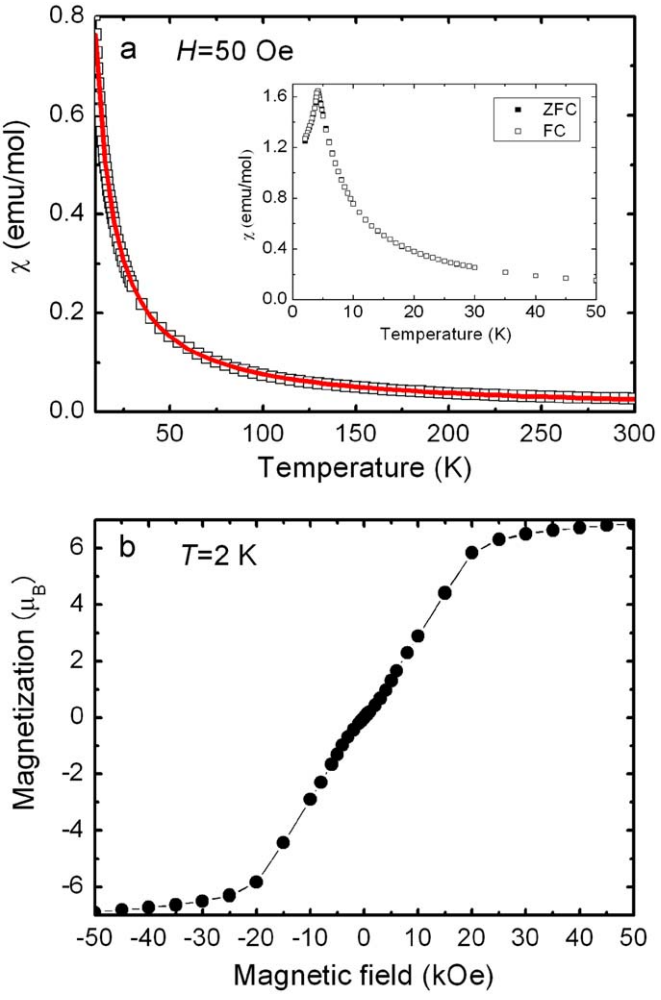

Fig. 4. (a) Temperature dependence of magnetic susceptibility of $EuZrO_3$ (open squares) measured in a magnetic field (H) of 50 Oe. The solid line represents the theoretical curve based on Eqs. (4)–(6). The inset shows both FC (open squares) and ZFC (closed squares) curves in the low temperature region. (b) Field dependence of magnetization of $EuZrO_3$ (closed circles) measured at 2 K. The solid line is a guide for the eye.

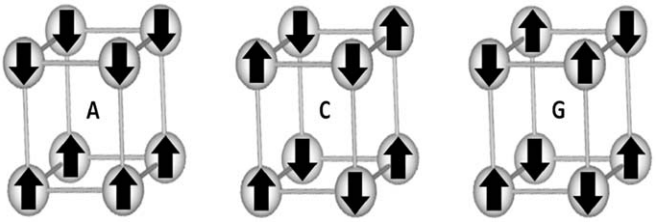

Fig. 5. Schematic depiction of the *A*-, *C*-, and *G*-type AFM structures. The arrows represent spin orientation in a cubic lattice.

structure for a series of Eu^{2+}-containing perovskite oxides may allow us to deduce the magnetic structure of $EuZrO_3$. A neutron diffraction study on cubic perovskite $EuTiO_3$ revealed a *G*-type AFM structure [4], and the analysis of molecular-field approximation on $EuTiO_3$ yielded $J_1/k=-0.014$ K and $J_2/k=+0.037$ K [5]. Greedan et al. [26] applied the molecular-field approximation to cubic perovskite $EuMg_{0.5}W_{0.5}O_3$ and $EuLu_{0.5}Ta_{0.5}O_3$, and compared the sets of exchange constants for *A*- and *G*-type with the J_1 and J_2 values obtained for $EuTiO_3$. They found that the J_1 and J_2 values vary systematically with the NN and NNN distances between Eu^{2+} ions, respectively, provided that the AFM structure for $EuMg_{0.5}W_{0.5}O_3$ and $EuLu_{0.5}Ta_{0.5}O_3$ is of *G*-type. Namely, the value of J_1/k decreases in the order of $EuTiO_3$ (-0.014 K), $EuMg_{0.5}W_{0.5}O_3$ (-0.030 K for *G*-type), and $EuLu_{0.5}Ta_{0.5}O_3$ (-0.095 K for *G*-type), which is the order of increasing NN Eu^{2+}-Eu^{2+} distance: $EuTiO_3$ (3.904 Å), $EuMg_{0.5}W_{0.5}O_3$ (3.951 Å), and $EuLu_{0.5}Ta_{0.5}O_3$ (4.100 Å). The value of J_2/k also decreases in the order of $EuTiO_3$ (+0.037 K), $EuMg_{0.5}W_{0.5}O_3$ (+0.007 K for *G*-type), and $EuLu_{0.5}Ta_{0.5}O_3$ (-0.095 K for *G*-type), i.e., in the order of increasing NNN Eu^{2+}-Eu^{2+} distance: $EuTiO_3$ (5.521 Å), $EuMg_{0.5}W_{0.5}O_3$ (5.588 Å), and $EuLu_{0.5}Ta_{0.5}O_3$ (5.798 Å). In the case of $EuZrO_3$, the mean NN and NNN Eu^{2+}-Eu^{2+} distances (4.109 and 5.809 Å as seen from Table 2) are longer than those in $EuTiO_3$, respectively, so that the set of exchange constants for *G*-type ($J_1/k=-0.032$ K, $J_2/k=+0.017$ K) is more compatible with the variations of J_1 and J_2 values with NN and NNN Eu^{2+}-Eu^{2+} distances than that for *A*-type ($J_1/k=+0.033$ K, $J_2/k=-0.031$ K). Here, it should be noted that there exist differences in the set of exchange constants for the *G*-type AFM ordering between $EuLu_{0.5}Ta_{0.5}O_3$ and $EuZrO_3$ despite their similar NN and NNN Eu^{2+}-Eu^{2+} distances. This may be caused by the neglect of the structural distortion in $EuZrO_3$ involving the distribution of Eu–O–Eu bond angles during the above calculation. In addition, for orthorhombic perovskite $EuZrO_3$ with magnetic *A*-site ions, the presence of single-ion anisotropy and magnetic dipole–dipole interactions may lead to spin canting; however, the degree of spin canting should be considerably small in $EuZrO_3$ since Eu^{2+} is an *S*-state ion, which is similar to the case in orthorhombic perovskite $GdAlO_3$ where Gd^{3+} ions are in the same *S* ground state [27]. Further studies are required to clarify the magnetic structure in $EuZrO_3$.

4. Conclusion

In summary, perovskite $EuZrO_3$ was synthesized through a high temperature solid-state reaction. Through the Rietveld analysis of XRD data the crystal structure of $EuZrO_3$ was refined to orthorhombic perovskite (*Pbnm* space group) with lattice constants $a=5.79469(9)$, $b=5.82521(7)$, and $c=8.19799(14)$ Å. The analysis of ^{151}Eu Mössbauer spectrum indicates that almost all the europium ions are present as Eu^{2+} and occupy the distorted sites with non-axial electric field gradients. An AFM behavior of $EuZrO_3$ is observed below $T_N\sim4.1$ K with a positive θ_W of 0.07 K. The possible mechanism of the magnetic transition has been discussed.

References

[1] V.G. Zubkov, A.P. Tyutyunnik, V.A. Pereliaev, G.P. Shveikin, J. Köhler, R.K. Kremer, A. Simon, G. Svensson, J. Alloys Compd. 226 (1995) 24–30.
[2] K. Ishikawa, G. Adachi, J. Shiokawa, Mater. Res. Bull. 16 (1981) 419–427.
[3] G.K. Strukova, D.V. Shovkun, V.N. Zverev, I.E. Batov, S.A. Zver'kov, S.S. Khasanov, Physica C 351 (2001) 363–370.
[4] T.R. McGuire, M.W. Shafer, R.J. Joenk, H.A. Alperin, S.J. Pickart, J. Appl. Phys. 37 (1966) 981–982.
[5] C.L. Chien, S. DeBenedetti, F. De Barros, Phys. Rev. B 10 (1974) 3913–3922.
[6] R. Ranjan, H.S. Nabi, R. Pentcheva, J. Phys.: Condens. Matter. 19 (2007) 406217.
[7] T. Katsufuji, H. Takagi, Phys. Rev. B 64 (2001) 054415.
[8] K. Fujita, N. Wakasugi, S. Murai, Y. Zong, K. Tanaka, Appl. Phys. Lett. 94 (2009) 062512.
[9] T. Katsufuji, Y. Tokura, Phys. Rev. B 60 (1999) R15021–R15023.
[10] A.H. Shafer, J. Appl. Phys. 36 (1965) 1145–1152.
[11] V. Viallet, J.F. Marucco, J. Saint, M. Herbst-Ghysel, N. Dragoe, J. Alloys Compd. 461 (2008) 346–350.
[12] (a) H.M. Rietveld, Acta Crystallogr. 22 (1967) 151–152;
(b) A.C. Larson, R.B. Von Dreele, General Structure Analysis System (GSAS), Los Alamos National Laboratory Report LAUR, 2000, pp. 86–748.;
(c) B.H. Toby, J. Appl. Cryst. 34 (2001) 210–213.
[13] K. Momma, F. Izumi, J. Appl. Crystallogr. 41 (2008) 653–658.
[14] S. Sasaki, C.T. Prewitt, R.C. Liebermann, Am. Miner. 68 (1983) 1189–1198.
[15] M. Wakeshima, Y. Doi, Y. Hinatsu, J. Solid State Chem. 157 (2001) 117–122.
[16] J.M.D. Coey, A. McEvoy, M.W. Shafer, J. Non-Cryst. Solids 43 (1981) 387–392.
[17] B.A. Goodmen, N.N. Greenwood, G.E. Turner, Chem. Phys. Lett. 5 (1970) 181–182.
[18] G.K. Shenoy, B.D. Dunlap, Nucl. Instrum. Methods 71 (1969) 285–291.
[19] F. Grandjean, G.J. Long, in: G.J. Long, F. Grandjean (Eds.), Mössbauer Spectroscopy Applied to Inorganic Chemistry, vol. 3, Plenum Press, New York, 1989, pp. 513–597.
[20] K. Fujita, K. Tanaka, K. Hirao, N. Soga, J. Am. Ceram. Soc. 81 (1998) 1845–1851.
[21] O. Berkooz, J. Phys. Chem. Solids 30 (1969) 1763–1766.
[22] J.H. Van Vleck, The Theory of Electric and Magnetic Susceptibilities, Clarendon Press, Oxford, 1932, p. 248.
[23] L.M. Holmes, R. Sherwood, L.G. Van Uitert, Phys. Rev. 178 (1969) 576–579.
[24] T. Kasuya, IBM J. Res. Dev. 14 (1970) 214–223.
[25] J.E. Greedan, G.J. McCarthy, Mater. Res. Bull. 7 (1972) 531–542.
[26] J.E. Greedan, C.L. Chien, R.G. Johnston, J. Solid State Chem. 19 (1976) 155–160.
[27] D.C. Cook, J.D. Cashion, J. Phys. C: Solid State Phys. 13 (1980) 4199–4210.